Neurochemical Research (2024) 49:2021–2037
https://doi.org/10.1007/s11064-024-04153-5

ORIGINAL PAPER

Mechanism of Purinergic Regulation of Neurotransmission in Mouse Neuromuscular Junction: The Role of Redox Signaling and Lipid Rafts

Arthur R. Giniatullin[1] · **Kamilla A. Mukhutdinova**[1,2] · **Alexey M. Petrov**[1,2,3]

Received: 28 February 2024 / Revised: 16 April 2024 / Accepted: 16 May 2024 / Published online: 30 May 2024

Abstract

Acetylcholine is the main neurotransmitter at the vertebrate neuromuscular junctions (NMJs). ACh exocytosis is precisely modulated by co-transmitter ATP and its metabolites. It is assumed that ATP/ADP effects on ACh release rely on activation of presynaptic G_i protein-coupled P_2Y_{13} receptors. However, downstream signaling mechanism of ATP/ADP-mediated modulation of neuromuscular transmission remains elusive. Using microelectrode recording and fluorescent indicators, the mechanism underlying purinergic regulation was studied in the mouse diaphragm NMJs. Pharmacological stimulation of purinoceptors with ADP decreased synaptic vesicle exocytosis evoked by both low and higher frequency stimulation. This inhibitory action was suppressed by antagonists of P_2Y_{13} receptors (MRS 2211), Ca^{2+} mobilization (TMB8), protein kinase C (chelerythrine) and NADPH oxidase (VAS2870) as well as antioxidants. This suggests the participation of Ca^{2+} and reactive oxygen species (ROS) in the ADP-triggered signaling. Indeed, ADP caused an increase in cytosolic Ca^{2+} with subsequent elevation of ROS levels. The elevation of $[Ca^{2+}]_{in}$ was blocked by MRS 2211 and TMB8, whereas upregulation of ROS was prevented by pertussis toxin (inhibitor of G_i protein) and VAS2870. Targeting the main components of lipid rafts, cholesterol and sphingomyelin, suppressed P_2Y_{13} receptor-dependent attenuation of exocytosis and ADP-induced enhancement of ROS production. Inhibition of P_2Y_{13} receptors decreased ROS production and increased the rate of exocytosis during intense activity. Thus, suppression of neuromuscular transmission by exogenous ADP or endogenous ATP can rely on P_2Y_{13} receptor/G_i protein/Ca^{2+}/protein kinase C/NADPH oxidase/ROS signaling, which is coordinated in a lipid raft-dependent manner.

Graphical Abstract

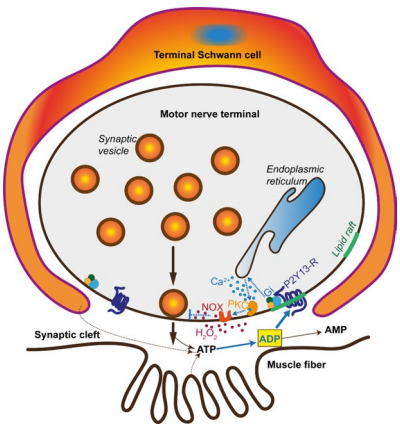

Keywords ATP · Acetylcholine · Neuromuscular junction · Lipid raft · Purinoceptor · Reactive oxygen species

Abbreviations

Ach	Acetylcholine
ADP	Adenosine diphosphate
ATP	Adenosine triphosphate
EPC	End-plate current
ChO	Cholesterol oxidase
NMJ	Neuromuscular junction

Extended author information available on the last page of the article

NOX	NADPH oxidase
MEPC	Miniature end plate current
PKC	Protein kinase C
ROS	Reactive oxygen species
SMase	Sphingomyelinase
SV	Synaptic vesicle

Introduction

Neuromuscular junction (NMJ) is a specialized chemical synapse, where axonal action potential is converted into activation of the muscle fiber. In vertebrate NMJs, the main neurotransmitter is acetylcholine (ACh), which is released from synaptic vesicles (SVs) and then activates postsynaptic nicotinic ACh receptors (nAChRs) leading to end plate depolarization. Several tens of SVs undergo exocytosis in response to single nerve stimulus at the mammalian NMJs, this number of ACh quanta significantly exceed that required to trigger an action potential on the sarcolemma [1, 2]. On the one hand, this ensures the reliability of neuromuscular transmission. On the other hand, excessive exocytosis can lead to depletion of SV pool during intense activity, since slow kinetics of vesicle endocytosis cannot keep up with the rate of exocytosis [3, 4]. In addition, excessive ACh release causes high energy expenditure [5] and even premature aging of NMJs [6]. Accordingly, negative feedback loops are vital for adaptation of neuromuscular transmission and limitation of ACh exocytosis. One of these loops is realized through the action on presynaptic receptors of co-transmitter molecules, which, along with ACh, are present in SV [7, 8].

ATP is the main co-transmitter of ACh in the vertebrate NMJs [7–9]. Over time, released ATP is enzymatically hydrolyzed to ADP, AMP and eventually adenosine in the synaptic cleft. ATP and ADP modulate neurotransmission via activation of inotropic P_2X-or (and) metabotropic P_2Y-purinoceptors, whereas adenosine acts though metabotropic adenosine (P_1) receptors [8]. ATP/ADP-dependent suppression of ACh release from vertebrate motor nerve terminals appears to be primarily due to activation of G_i protein-coupled P_2Y receptors, without marked contribution of P_2X receptors [9–13]. At the frog NMJs, ATP reduced ACh release acting via P_2Y_{12} receptors / NADPH oxidase (NOX)/reactive oxygen species (ROS) axis [9, 10, 13]. Generated ROS might inhibit ACh release by affecting the exocytotic protein SNAP-25 [14] or ROS-sensitive signaling molecules and ion channels in the frog NMJs [15, 16]. At the mouse NMJs, P_2Y_{13} receptors mediated adenine nucleotides-dependent presynaptic inhibition of ACh release [11, 17]. This receptor subtype was identified in the presynaptic motor nerve terminals of mouse diaphragm [11]. However, a downstream signaling mechanism of P_2Y_{13} receptor-driven regulation of neurotransmission in the mammalian NMJs remains elusive.

Given the relationship between P_2Y_{13} receptors and lipid trafficking [18–20], functioning of these receptors can be dependent on a lipid microenvironment, specifically lipid raft stability. Lipid rafts are abundant in the NMJ membranes [21–24] and the junctional lipid raft disturbance was observed after short-term muscle disuse [25, 26] and at the early stage in models of amyotrophic lateral sclerosis [27, 28].

In the present study, we tested the hypothesis that NOX-derived ROS is a key element in purinergic regulation of neurotransmitter release at the mouse NMJs. Additionally, the relevance of Ca^{2+} signaling and lipid microenvironment for purinergic regulation of exocytosis was assessed. We demonstrated that exogenous (ADP) and endogenous purines acting on P_2Y_{13} receptors suppress ACh exocytosis, causing a rapid Ca^{2+} release from intracellular stores, protein kinase C activation, NOX-mediated generation of ROS. The integrity of lipid raft components, cholesterol and sphingomyelin, is required for P_2Y_{13} receptor-dependent attenuation of SV exocytosis.

Methods

Ethical Approval and Animals

Animal care and experiments were carried out in accordance with the NIH Guide for the Care and Use of Laboratory Animals and the EU Directive 2010/63/EU. The experimental protocol was approved by the Local Ethical Committee of Kazan Medical University (Protocol #1/January 25, 2022) and Kazan Federal Scientific Centre (#23/7; May 12, 2023). All efforts were made to minimize animal suffering. BALB/c mice were housed at a 12-h light/12-h dark cycle in ventilated cages at temperature and humidity-controlled environment with free access to food and water. Animals were not intentionally randomized and investigators were not blinded to the nature of chemicals used. After anesthesia of mice (both sexes, 4–5-month-old), diaphragm with phrenic nerve stubs was quickly excised and hemidiaphragm-phrenic nerve preparations were placed into experimental chambers. The hemidiaphragm was attached to Sylgard-coated bottom of the chamber (total volume of 5 ml) and the phrenic nerve stub was loosely drawn into a suction electrode.

Solutions and Chemicals

The nerve-muscle preparations were continuously perfused at 5 ml/min with physiological solution (pH-7.4) containing (in mM): 120NaCl, 5KCl, $2CaCl_2$, $1MgCl_2$, $1NaH_2PO_4$, $24NaHCO_3$, 11 glucose; the solution was saturated with

carbogen (5% CO_2 and 95% O_2 mixture). These reagents were purchased from Sigma. In some experiments, modified physiological solution, containing high K^+ (40 mM KCI; NaCI concentration was decreased to keep normal osmolarity, 310 ± 5 mOsm/L) was used. The osmolarity was measured using an OSMOMAT 3000 Osmometer (Gonotec GmbH). In electrophysiological experiments, the muscle fibers were cut transversely ('cut muscles') to prevent muscle contractions and to simultaneously maintain the physiological level of quantal release and cable properties [29]. In the cut muscles, recording began after the stabilization of membrane potential (i.e., ~ 50–60 min after the cutting procedure). In fluorescent experiments, the contractions were blocked by 15 min pre-exposure to inhibitor of postsynaptic nicotinic ACh receptor antagonist d-tubocurarine (2 µM; Cat. # 5.05145, Sigma).

Application of neutral sphingomyelinase (SMase; 0.01 U/ml; Cat. # S9396; Sigma), which partially disrupts junctional lipid rafts by hydrolyzing membrane sphingomyelin, lasted 15 min [30]. Another lipid raft destabilizing enzyme cholesterol oxidase (ChO, 0.2 U/ml; Cat. # 228,250, Sigma) was also applied for 15 min [31]. To inhibit $G_{i/o}$ protein, mice were injected by pertussis toxin (PTX; Cat. # 70,323–44-3, Sigma) at dose of 150 µg/kg (in sodium-phosphate buffer) 72 h before the experiments [32]. The following chemicals were used: 10 µM ADP (an agonist of P_2Y_1-, P_2Y_{12}-, P_2Y_{13}-receptors; Cat. # 01905, Sigma), 100 µM IDP/inosine 5′-diphosphate sodium salt (a preferential agonist for P_2Y_{13}-receptors; Cat. # NI10027, Biosynth), MRS 2211 (an antagonist of P_2Y_{13}-receptors, 10 µM; Cat. # 2402, Tocris), 1 mM N-acetylcysteine/NAC (an antioxidant; Cat. # A7250, Sigma), 1200 U/ml catalase (an antioxidant enzyme; Cat. # C9322, Sigma), 1 µM chelerythrine chloride (protein kinase C inhibitor; Cat # C-400, Alomone labs), 10 µM TMB8 (an inhibitor of intracellular calcium mobilization; Cat. # T111, Sigma). MRS 2211, NAC, catalase, chelerythrine and TMB8 were added to the bathing solution 30 min before P_2Y agonist administration and remained in perfusion throughout the experiment. All chemicals were dissolved to the final concentrations in working solution immediately before use.

Electrophysiological Recordings

Recording of the postsynaptic end-plate currents (EPCs) and miniature EPCs (MEPCs) were performed using standard two-electrode voltage-clamp technique described previously in details [33, 34]. Briefly, two intracellular sharp borosilicate-glass microelectrodes (tip diameter of ~ 1 µm, 4–5 MΩ resistance) filled with 2.5 M KCl were impaled into the junctional region with interelectrode distance of ~100 µm. MEPCs and EPCs were detected using Axoclamp 900 A amplifier (Molecular devices, USA) and LA 2 digital I/O board (Rudnev-Shelyev, Moscow, Russia). In the case of EPC recordings, the value of postsynaptic membrane potential was maintained at − 45 mV (leak currents were in the range of 10–20 nA). EPCs were evoked by supra-threshold stimuli (duration of 0.1 ms) at 0.05 Hz. The stimuli were applied to the phrenic nerve via a suction electrode connected to DS3 stimulator (Digitimer Ltd., UK). Recordings of MEPCs were performed on intact muscles with the resting membrane potentials maintained at − 60 mV; signal-to-noise ratio was > 5:1 and threshold for the MEPC detection was set at a level of 2 nA. In case of MEPC recordings, no less than 8 muscle fibers were studied in each animal. Amplitudes, 20–80% rise time, and half decay time (from the peak to 50%) of MEPCs and EPCs were calculated. The signals were digitized at 50 kHz and analyzed off-line using Elph software [35].

Estimation the Rate of Synaptic Vesicle Exocytosis at Intense Activity

The rate of SV exocytosis was assessed using FM1-43 dye, as described previously in details [33, 36]. Briefly, FM1-43 dye (Cat. # T-35356, Thermo Fisher Scientific) reversibly binds to surface membranes and is then taken up by endocytosis into SVs. Next, nerve stimulation causes exocytotic release of FM1-43 from SVs [37]. To load FM1-43 into SVs, phrenic nerve was stimulated at 20-Hz for 1 min, thereby triggering massive SV exocytosis following endocytosis. FM1-43 (7 µM) was present in the external solution ½ min before 20 Hz stimulation, during stimulation and 5 min after the end of stimulation. Next, the muscles were washed for 20 min with dye-free physiological saline containing 20 µM ADVASEP-7 (Cat. # 70,029; Biotium). The latter facilitates the dissociation of FM1-43 from the surface membrane. Dye-loaded nerve terminals were treated with chemicals and re-stimulated at 20 Hz for 10 min to provoke SV exocytosis, leading to FM1-43 release from SVs ("unloading" or "destaining"). Fluorescence of FM1-43 was excited by a 480/10 nm light, and emission was recorded using a 535/40 nm filter.

FM1-43 fluorescence ($\Delta F = F_{ROI}\text{-}F_{back}$) was calculated in nerve terminals as a mean pixel intensity (in arbitrary units, a.u.) after background signal subtraction (F_{back}), which was determined in a region (4×30 µm^2) outside the nerve terminals. A value of nerve terminal fluorescence (immediately before unloading stimulation; ΔF_{max}) was set as 1.0 and a ratio of $\Delta F/\Delta F_{max}$ was calculated during the unloading stimulation at 20 Hz. $\Delta F/\Delta F_{max}$ did not change under resting conditions for 10 min (without nerve stimulation).

Fluorescence was detected using high-sensitive cameras, Dhyana 400BSI V2 (Tucsen) or DP72 (Olympus), and BX51WI microscope equipped by confocal disk scanning unit (Olympus) and CoolLED pE-4000 light source (CoolLED Ltd.). The cameras were controlled by Mosaic

(Tucsen) and Cell P (Olympus) software. The regions containing NMJs were illuminated only at the moments of image recording (< 1 second). Image Pro software (Media Cybernetics) was used to analyze fluorescence intensity.

Intracellular ROS Imaging

Detection of cytosolic ROS in NMJs was carried out using CM–H2DCFDA (#C6827; ThermoFisher Scientific) as described previously [34]. CM–H2DCFDA permeates the cells, and becomes trapped in the cytoplasm after hydrolysis by intracellular esterases. Muscles were exposed to 5 µM CM–H2DCFDA for 30 min, rinsed for 50 min with dye-free physiological solution and visualized with Olympus BX51 fluorescent microscope. CM–H2DCFDA fluorescence was evoked by a light of wavelength at 480/15 nM and the emission was recorded using a 505–550 nm band-pass filter. Excessive illumination was strictly avoided and preparations characterized by unstable fluorescence under basal conditions were excluded. Sample illumination was limited to 9 frames at 5 min intervals for 40 min to minimize photo-oxidation of the dye. This protocol allows to overcome the limitations of the dye [38, 39]. The intensity of fluorescence was quantified using Image Pro software and relative changes in fluorescence from baseline were estimated as previously described [34].

Measurements of Extracellular H_2O_2

The extracellular H_2O_2 levels were estimated with Amplex Red Hydrogen Peroxide/Peroxidase Assay Kit (Cat. # A22188; ThermoFisher Scientific) as described previously [32, 34]. Briefly, in the presence of horseradish peroxidase Amplex Red reagent (10-acetyl-3,7-dihydroxyphenoxazine) reacts with H_2O_2 (stoichiometry of 1:1) to produce resorufin, the stable red-fluorescent product. Basal levels of H_2O_2 were estimated after exposure of the preparation for 15 min to physiological saline (total volume of 400 µl) containing 100 µM Amplex Red reagent and 0.2 U/ml horseradish peroxidase. The bathing solution was mixed constantly by a recirculating mechanism. Then, the bathing solution was collected, stored for 50 min in the dark at room temperature and fluorescence was recorded. The fluorescence of resorufin was excited by 535/10 nM and the emission was detected at 590 nM. Background fluorescence derived from non-H_2O_2 reactions was subtracted from each value. For calibration a set of physiological solution with different H_2O_2 concentrations was used.

Assessment of Cytosolic Ca^{2+} Changes

Estimation of cytosolic Ca^{2+} changes in synaptic regions was performed using Oregon Green 488 BAPTA-1 (Cat. # O6807, Thermo Fisher Scientific) as described previously [32]. This is a cell-permeable high-affinity Ca^{2+} indicator (K_d ~ 170 nM) which allows to record small changes in cytosolic Ca^{2+} content near the resting levels. The preparations were incubated for 20 min with 2 µM Oregon Green 488 BAPTA-1 and then rinsed for 40 min with dye-free physiological solution. Finally, recording of fluorescence in synaptic regions were performed. Fluorescence was evoked by 1-s light flashes at 488/10 nm and the emission was detected with a 505–550 nm band-pass filter. The value of fluorescence before chemical application was set to 1.0.

Statistics

OriginPro software was used for statistical analysis. Data are represented as mean ± standard deviation (SD); all exceptions are indicated (Fig. 3A, B). Sample size (n) is a number of independent experiments on individual animals and it was chosen based on a reasonable value of SD; sample size is denoted on each figure legend. Normality and variance homogeneity were tested by Shapiro–Wilk test and two-sample F test for variance, respectively. Statistical significance was assessed by a two-tailed paired *t*-test (for parametric and paired data) and Mann–Whitney *U* test (for comparison of two unpaired groups). Values of $^*P < 0.05$, $^{**}P < 0.01$, $^{***}P < 0{,}001$ were considered as significant.

Results

P_2Y_{13} Receptors are Involved in Regulation of Spontaneous Exocytosis and Evoked Neurotransmitter Release at Low Frequency Stimulation

Previously, it was found that G_i protein-coupled P_2Y receptors implicated in presynaptic inhibition of spontaneous and evoked ACh release belong to P_2Y_{13} subtype at the mouse motor nerve terminals [11, 40]. Rodent P_2Y_{13} receptors are activated by both ADP and IDP [41, 42]. Expectedly, ADP (10 µM) and IDP (100 µM) reversibly reduced the amplitude of EPCs elicited by low-frequency (0.05 Hz) stimulation of the phrenic nerve (Fig. 1A, B).

By 15th min of ADP or IDP administration the EPC amplitude decreased by 29 ± 8% (n = 11, p = 0.003) or 37 ± 9% (n = 8, p = 0.007), respectively (Fig. 1 A, B). Under these conditions, the EPC kinetics (assessed by rise and decay time) was not affected (Fig. 1C, D). MRS 2211 (10 µM), a selective P_2Y_{13} receptor antagonist, completely prevented the inhibitory effect on EPC amplitude of both ADP and IDP (Fig. 1A, B). Importantly, that MEPC amplitude as well as rise and decay time, indicators of postsynaptic membrane sensitivity to ACh, were not changed upon

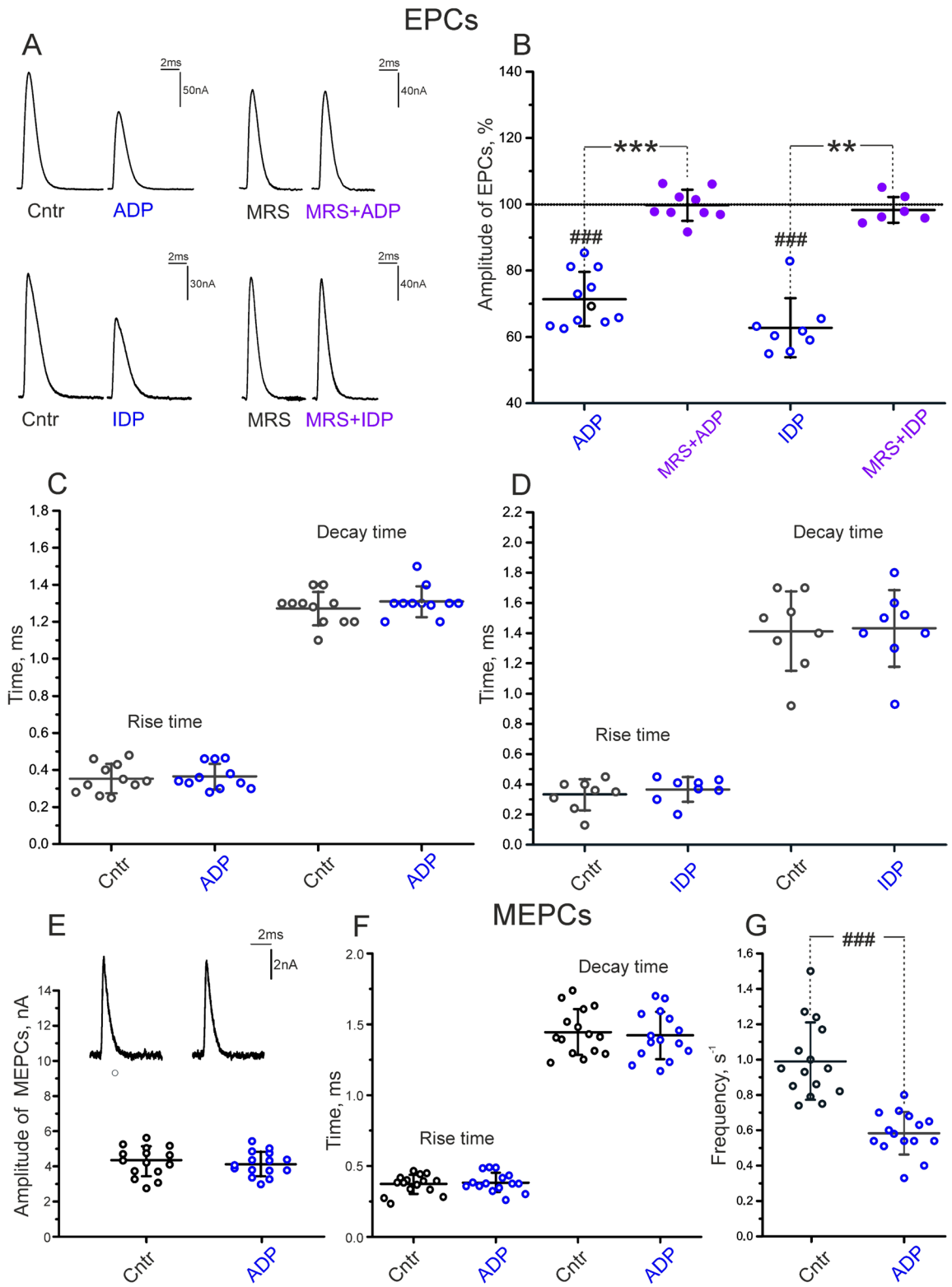

Fig. 1 Influence of ADP and IDP on evoked and spontaneous neurotransmitter release. **A** Representative multiquantal EPCs before and 15 min after addition of 10 μM ATP or 100 μM IDP in control and after treatment with 10 μM MRS 2211 (MRS). **B** Histograms showing the action of ADP (n = 11 mice) and IDP (n = 8) in control, and in the presence of MRS 2211 (n = 6). **C**–**D** Rise and decay time of EPCs before and after treatment with ADP (**C**) and IDP (**D**). **E**–**G** Graphs show amplitude values and the representative traces of MEPCs (**E**), rise and decay time (**F**) as well as frequency of MEPCs (**G**) before and after treatment with 10 μM ADP. n = 15. **B**–**G**: $^{**}P < 0.01$, $^{***}P < 0.001$—by a Mann–Whitney *U* test between groups; $^{\#\#\#}P < 0.001$ by two-tailed *t*-test as compared to pretreatment baseline

ADP application (Fig. 1E, F). At the same time, MEPC frequency decreased from 1.0 ± 0.2 to 0.6 ± 0.1 s^{-1} ($p < 0{,}001$; n = 15) by 15th min of ADP administration (Fig. 1 G). Thus, ADP via activation of P_2Y_{13}-receptors suppressed both spontaneous exocytosis and evoked neurotransmitter release upon single stimuli in the mouse NMJs.

Purinoceptor-Dependent Modulation of the Rate of Synaptic Vesicle Exocytosis During Intense Activity

During quiet breathing phrenic motor neurons discharge at 20–30 Hz [43]. This stimulation mobilizes SVs from different pools in the NMJs [44, 45]. Moreover, the efficiency of neurotransmission at intense activity depends mainly on SV delivery to active zone and their recycling [46, 47]. In this section, using FM1-43 dye, we tested the contribution of purinergic receptors in regulation of SV recruitment into exocytosis during prolonged nerve stimulation at 20 Hz (Fig. 2).

Motor nerve terminals were loaded with fluorescent FM1-43 dye by 20 Hz stimulation for one minute. Then, preloaded nerve terminals were re-stimulated at 20 Hz to induce the exocytotic dye release (unloading) in control and after treatment with chemicals (Fig. 2A–C). ADP (10 µM) decreased the rate of FM1-43 unloading during 20 Hz activity (Fig. 2A). As a result, 27 ± 20% ($p = 0.006$, n = 11) and 31 ± 12% ($p < 0.001$) less dye was released by 60 and 600 s of the stimulation, respectively, as compared to control (Fig. 2D). A competitive antagonist of P_2Y_{13} receptors, MRS 2211 (10 µM), enhanced the rate of FM1-43 unloading (Fig. 2B), causing an increase in FM1-43 dye portion release by 54 ± 21% ($p < 0.001$, n = 7) and 15 ± 5% ($p = 0.003$) after 60 and 600 s of the stimulation, respectively (Fig. 2D). In the presence of MRS 2211, the suppressive effect of ADP on exocytotic dye release was markedly reduced (Fig. 2B) and the dye loss was only by 15 ± 17% ($p = 0.053$, n = 10) less after 600 s of stimulation as compared to control (Fig. 2D).

Thus, exogenous ADP acting mainly via P_2Y_{13} receptors suppressed SV involvement in exocytosis during prolonged 20 Hz activity. Activation of P_2Y_{13} receptor by endogenous ATP released at intense activity can contribute to negative regulation of the rate of SV exocytosis.

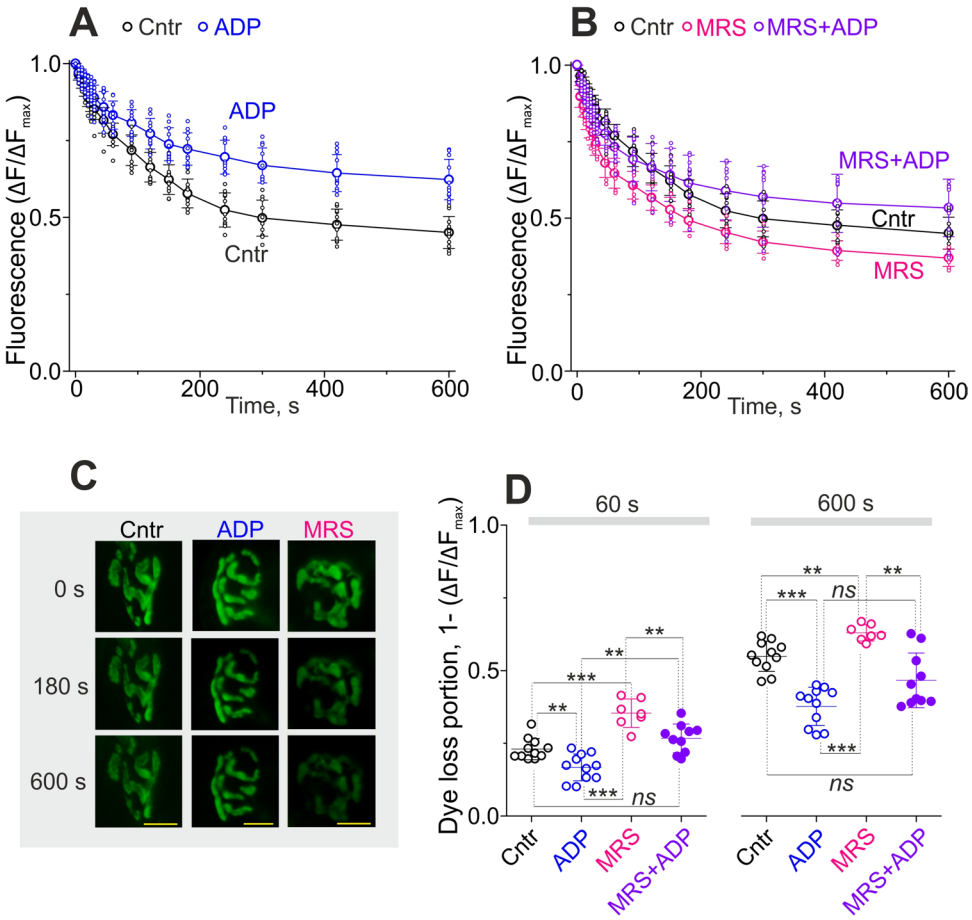

Fig. 2 Purinergic regulation of synaptic vesicle recruitment to exocytosis during phrenic nerve stimulation at 20 Hz. **A**, **B** The kinetics of FM1-43 dye unloading from motor nerve terminals in control (Cntr), after treatment with ADP, P_2Y_{13}-receptor antagonist MRS 2211 (MRS), and ADP in the presence of MRS 2211. n = 11 (Cntr), 11 (ADP), 7 (MRS) and 10 (MRS + ADP). **C** Representative fluorescent images immediately before (0) and at different time points (180 and 600 s) of unloading stimulation. Scale bars—15 µm. **D** Quantification of dye loss portions by 60 and 600 s of stimulation; data calculated from **A** and **B**. **P < 0.01, ***P < 0.001 by a Mann–Whitney *U* test between groups; *ns* non significant. **A**, **B** and **D**: data are represented as mean ± SD

The Contribution of Purinoceptors to ROS Production: Signaling Pathways

Assessment of Cytoplasmic ROS Levels

ROS imaging using the CM-H2DCFDA dye, which upon oxidation by intracellular ROS forms highly fluorescent carboxy-dichlorofluorescein, provided further insights into the mechanism of ATP/ADP action. 15-min application of 10 μM ADP markedly increased CM-H2DCFDA fluorescence by 177 ± 88% (n = 13, p < 0.001) in the synaptic regions. (Fig. 3A, B). This enhancement of cytosolic ROS began with a 5-min lag period after the addition of ADP. Hypothetically, lipid rafts may be involved in ADP-mediated elevation of ROS. Previously, we found a functional coupling of P_2Y_{12}-receptor/NOX axis to lipid rafts at the frog NMJs [9]. Sphingomyelin-hydrolyzing enzyme SMase at low concentration (0.01 U/ml) can disrupt the lipid rafts mainly in synaptic zones of mouse NMJs [30]. SMase preapplication completely eliminated the ADP effect on CM-H2DCFDA fluorescence (Fig. 3B). An increase in CM-H2DCFDA fluorescence was also observed during 20 Hz stimulation of the phrenic nerve. By 1st, 5th and 10th min of the stimulation, the fluorescence intensity was 116 ± 18% (n = 10, p = 0.01), 164 ± 39% (p < 0.001) и 222 ± 68% (p < 0.001) of the pre-stimulation value, respectively (Fig. 3 C, D). This may be explained by the effect of sufficient amounts of endogenous ATP released from nerve terminals during intense activity [48]. CM-H2DCFDA allows to detect the time course of ROS production but has certain limitations [38].

The main signaling form of ROS is H_2O_2, which has a relatively long half-life in living cells and can cross cell membranes [49–51]. Therefore, a specific sensor for extracellular H_2O_2 was used in further experiments.

Evaluation of Extracellular Levels of H_2O_2

The levels of extracellular H_2O_2 were estimated using the Amplex Red Hydrogen Peroxide/Peroxidase Assay Kit [9, 34]. 15 min application of ADP (10 μM) increased the extracellular content of H_2O_2. The fluorescence of resorufin, the product of Amplex Red reagent oxidation by H_2O_2, was elevated by 40 ± 36% (n = 7; p < 0.002) after ADP treatment (Fig. 3E).

Plasmalemmal NOX, a possible source of ROS, produces mainly extracellular superoxide radical anion, which is dismutated into H_2O_2 [52]. ADP-induced enhancement of resorufin fluorescence was prevented by VAS 2870 (10 μM), a selective inhibitor of NOX, as well as inhibition of Gi protein with PTX (150 μg/kg) (Fig. 3F). Hence, ADP, acting on Gi protein-coupled P_2Y receptors, increased H_2O_2 production involving NOX.

To test production of extracellular H_2O_2 during neuromuscular transmission, massive SV exocytosis was induced by either motor nerve stimulation (20 Hz) or membrane depolarization (by high K^+-containing saline) for 15 min. In both cases, resorufin fluorescence increased by 93 ± 12% (n = 4) and 27 ± 3% (n = 6, p < 0.001), respectively (Fig. 3F). These data are consistent with the assessment of the increase in intracellular ROS levels in response to motor nerve stimulation (Fig. 3C, D). As with the ADP effect, the nerve stimulation-induced enhancement of H_2O_2 levels was precluded by Gi protein blockage (Fig. 3F). Importantly, that P_2Y_{13} antagonist MRS 2211 profoundly suppressed the depolarization-induced elevation of resorufin fluorescence (Fig. 3F) and under these conditions the fluorescence increased only by 11 ± 1% (n = 6; p = 0.004).

Taken together, these data (3.3.1 and 3.3.2 sections) suggest that purinoreceptor activation with ADP enhances ROS production in a lipid raft, Gi protein and NOX-dependent manner. Intense synaptic activity also can increase ROS generation, at least in part, via activation of P_2Y_{13} receptors and Gi protein.

Contribution of ROS-Related Signaling in Purinergic Regulation of the Evoked Neurotransmitter Release at Low Frequency Stimulation

Next, we tested the action of ADP in the presence of several antioxidants known to prevent the cellular effects of ROS. First, we used 1 mM *N*-acetylcysteine (NAC), a membrane-permeable antioxidant, which itself increased the EPC amplitude to 136 ± 14% (n = 5). Pretreatment with NAC significantly reduced the negative action of 10 μM ADP (Fig. 4). By 15th min of ADP application, the EPC amplitude decreased only by 10 ± 8% (p < 0.001, n = 9), while in control the decline of EPC amplitude was approximately 3 times more pronounced (p < 0.001, n = 11). To explore the nature of the ROS which could be involved in the action of ADP, catalase, a non-membrane permeable enzyme which specifically destroys H_2O_2, was applied. In our experiments 1200 U/ml catalase increased the amplitude of EPCs by 14 ± 5% (p < 0.05, n = 6) and significantly reduced the inhibitory action of 10 μM ADP (Fig. 4). In the latter case, ADP decreased the EPC amplitude by 7 ± 7% (p < 0.001; n = 10). These results suggest the involvement of ROS, specifically extracellular H_2O_2, in the action of ADP on evoked neurotransmitter release.

Probably, the main source of ROS associated with the synaptic action of ADP could be NOXs. Indeed, pretreatment with NOX inhibitor VAS2870 significantly reduced the negative action of 10 μM ADP and 15 min after ADP addition the EPC amplitude decreased only by 11 ± 2% (Fig. 4). Molecular link between Gi protein coupled P_2Y_{13} receptor and activation of NOX can be protein kinase C (PKC) [53].

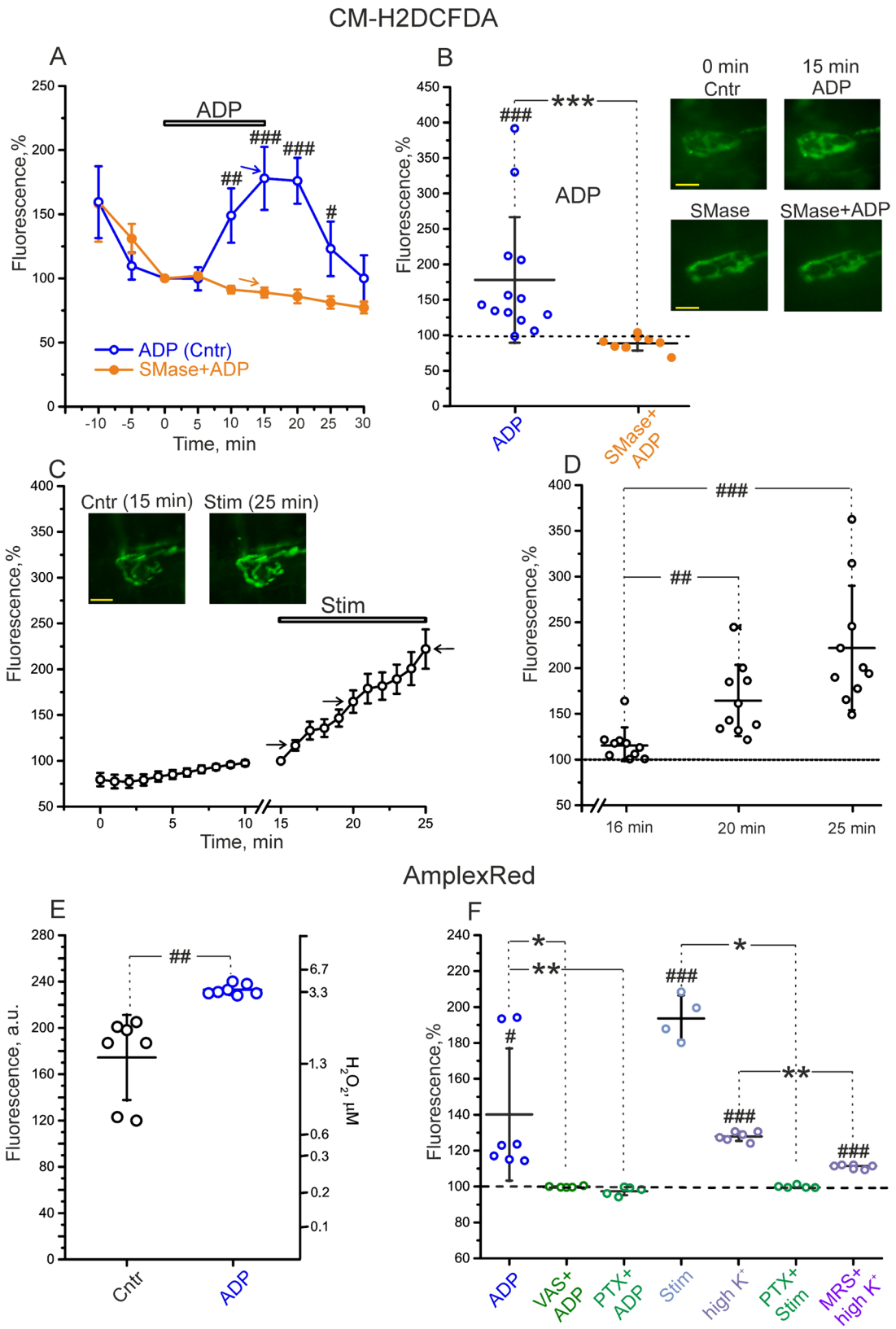
CM-H2DCFDA
A
ADP
Fluorescence, %
Time, min
ADP (Cntr)
SMase+ADP
B
0 min
Cntr
15 min
ADP
SMase
SMase+ADP
ADP
SMase+ ADP
C
Cntr (15 min)
Stim (25 min)
Stim
Time, min
D
16 min
20 min
25 min
AmplexRed
E
Fluorescence, a.u.
H2O2, μM
Cntr
ADP
F
VAS+ ADP
PTX+ ADP
Stim
high K+
PTX+ Stim
MRS+ high K+

◂**Fig. 3** ADP increases production of ROS. **A** Time course of ADP action on fluorescence of ROS-sensitive dye (CM-H2DCFDA) at junctional regions in control and after SMase preexposure. **B** Quantification of changes in CM-H2DCFDA fluorescence after 15 min exposure to ADP in control (n = 13) and SMase-pretreated samples (n = 8). Right, typical fluorescence images in control and after treatment with ADP alone and SMase + ADP. **A**, **B** The values immediately before ADP administration were set as 100%. **C** Time course of CM-H2DCFDA fluorescence in junctional regions before (0–15 min) and during (15–25 min) stimulation (10 min, 20 Hz) of phrenic nerve. Inserts, the representative fluorescent images captured at different time point before (15 min) and after (25 min) the stimulation. **D** Quantification of changes in CM-H2DCFDA fluorescence by 1st (16 min), 5th (20 min) and 10th min (25 min) of stimulation. **C**, **D** Values immediately before onset of the stimulation were set as 100%. **E** Action of ADP on levels of extracellular H_2O_2, detected by Amplex Red-based assay (n = 7). Control (cntr) indicates values before ADP application (in a.u.). The fluorescence was compared to H_2O_2 calibration curve to evaluate the levels of H_2O_2 (right Y axis). **F** Quantification of relative changes in resorufin fluorescence after ADP application in control (n = 7), after pretreatment with VAS 2870 (n = 5) and applying PTX (n = 6). Also, the effects of phrenic nerve stimulation (20 Hz, 15 min, n = 4) or high K^+-induced membrane depolarization (40 mM K^+, 15 min, n = 6) itself and in combination with PTX (n = 5) or MRS 2211 (n = 6) treatment are shown. **B**, **C**: Scale bars – 15 µm. **A**, **C** and **B**, **D**, **E**, **F** data are represented as mean ± SE and ± S.D, respectively. $^{\#}P < 0.05$, $^{\#\#}P < 0.01$, $^{\#\#\#}P < 0.001$ by paired two-tailed *t*-test as compared to baseline; $^{**}P < 0.01$, $^{***}P < 0.001$—by a Mann–Whitney *U* test between groups

The latter may be activated via Gi protein/Gβγ/phospholipase C pathway [32, 54, 55]. Cell-permeable protein kinase C inhibitor chelerythrine chloride (Chele), completely suppressed the effect of ADP on the EPC amplitude (Fig. 4). Note that ADP-dependent ROS generation was prevented by lipid raft-disrupting manipulation, particularly SMase pretreatment (Fig. 2A, B). Similarly, SMase markedly attenuated ADP-induced suppression of the EPC amplitude (Fig. 4).

Involvement of PKC and NADPH Oxidase in Purinergic Regulation of the Exocytotic Rate at Intense Activity

Here we tested the involvement of NOX and PKC in the ADP-mediated suppression of SV exocytosis during intense activity (20 Hz, 10 min). Inhibitor of NOX itself decreased the rate of FM1-43 unloading *vs* control (Fig. 5A, C). After inhibition of NOX, ADP lost its ability to decrease the exocytotic FM1-43 release and, conversely, increased the rate of FM1-43 destaining as compared to VAS2870-treated NMJs (Fig. 5A, C). As a result, 43 ± 14% (n = 8, $p < 0.001$) more dye was released for 600 s of 20 Hz stimulation in VAS + ADP *vs* VAS-treated NMJs (Fig. 5C). Inhibition of PKC, which can be responsible for NOX activation, did not modify FM1-43 dye unloading (Fig. 5B), but completely prevented ADP-mediated changes in the rate of FM1-43 release and, hence, amount of dye loss during 20 Hz stimulus train (Fig. 5B, C). Hence, ADP-induced activation of NOX in a PKC-dependent manner can mediate the negative effect of P_2Y_{13} receptors on SV recruitment to exocytosis at intense activity.

Purinergic Regulation of Cytosolic Ca^{2+}

PKC-dependent NOX activation can require calcium release from intracellular store [56]. We hypothesize that ADP, via P_2Y_{13}-receptors, may cause a rapid elevation of cytosolic Ca^{2+} before activation of NOX causing ROS generation, which begins with a 5-min delay after the addition of ADP. Indeed, application of ADP led to a rapid increase in intracellular Ca^{2+} levels in synaptic regions (Fig. 6A, D). The fluorescence of Oregon Green® 488 BAPTA-1 increased by 27 ± 4% (n = 8, p = 0.001) within the first 3 min of ADP administration. This rise in the fluorescence was completely prevented by both P_2Y_{13} receptor antagonist MRS 2211 (10 µM) (Fig. 6B, D) and inhibitor of Ca^{2+} release from endoplasmic reticulum TMB8 (10 µM) (Fig. 6C, D). Furthermore, TMB8 completely prevented the ADP-mediated suppression of exocytotic FM1-43 dye release upon prolonged 20 Hz stimulation (Fig. 6E, F). TMB8 itself slightly attenuated FM1-43 unloading and 16 ± 12% less dye (n = 7, p = 0.014) was released after 600 s of 20 Hz stimulation as compared to control (Fig. 6F). Thus, the elevation of cytosolic Ca^{2+} due to its release from intracellular store is an early event in P_2Y_{13} receptor-dependent signaling and required for ADP-induced suppression of SV involvement into exocytosis.

The Role of Lipid Raft Component in Purinergic Regulation of Synaptic Vesicle Involvement to Exocytosis

Sphingomyelin and cholesterol are building blocks for plasmalemmal microdomains, lipid rafts [57]. Enzymatic sphingomyelin hydrolysis (by SMase) and cholesterol oxidation (by ChO) were used to modulate the membrane properties, interfering with lipid raft signaling [58–60]. In addition, SMase treatment causes accumulation of ceramide, an active lipid and a player in neurological pathologies, at the plasmalemma [61]. Previously, we demonstrated that SMase (0.01 u/ml) and ChO (0.2 u/ml) partially disrupt lipid raft phase mainly in NMJ regions and enhance SV mobilization [30, 31]. Consistent with these data, SMase and ChO increased the rate of FM1-43 unloading (Fig. 7). After SMase pretreatment, the suppressive effect of ADP on FM1-43 unloading was attenuated (Fig. 7A, D), whereas action of P2Y13 receptor inhibitor was even inverted (Fig. 7B vs Fig. 2B), and MRS 2211 suppressed exocytotic FM-dye release during 20 Hz nerve stimulation (Fig. 7B). Indeed, 21 ± 6% less (n = 7,

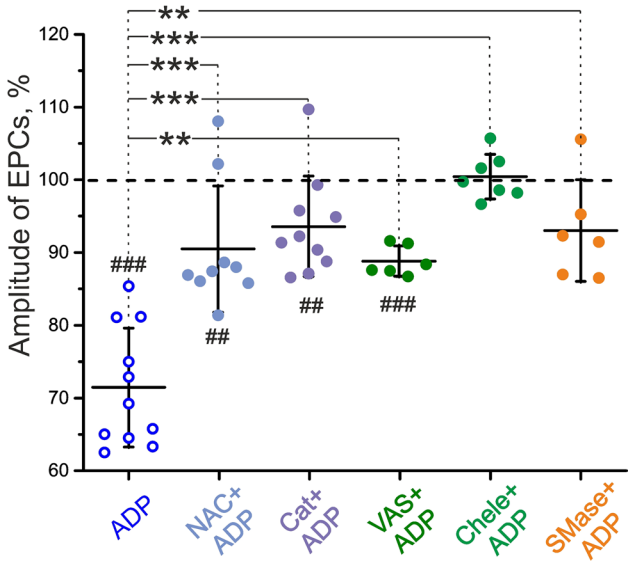

Fig. 4 Testing the role of ROS, NOX, PKC and lipid microenvironment in the action of ADP. Histogram shows effects (in %) of ADP on amplitude of EPCs in control and after pre-exposure to *N*-acetylcysteine (NAC) (n = 9), catalase (n = 10), VAS2870 (n = 6), chelerythrine (Chele) (n = 7) and 0.1 U/ml SMase (n = 6). **P < 0.01, ***P < 0.001—by a Mann–Whitney *U* test between groups. ##P < 0.01, ###P < 0.001 by paired two-tailed *t*-test as compared to value before ADP addition

p = 0.001) FM1-43 dye was released by 600 s of 20 Hz stimulation in SMase + MRS 2211 *vs* SMase-treated NMJs (Fig. 7D). Similarly, following ChO pretreatment MRS 2211 lost its ability to increase the rate of FM1-43 unloading (Fig. 7C, D).

Discussion

A large body of literature shows that extracellular nucleotides play an important role in intercellular signaling engaging inotropic (P_2X) and metabotropic (P_2Y) receptors in the nervous system [7, 8, 62]. Among metabotropic receptors, P_2Y_{13} subtype is one of the most recently cloned [63] and, together with the P_2Y_1 and P_2Y_{12} subtypes, P_2Y_{13} receptors belong to a distinct structural branch of the P_2Y receptors, which are more specific for ADP *vs* ATP [64]. In addition, P_2Y_{13} as well as P_2Y_{12}, and P_2Y_{14} receptors are coupled preferentially to Gi protein [63, 65].

P_2Y_{13} receptors seem to play an essential role in nervous system. Investigation of P_2Y_{13} receptor distribution in rat tissues demonstrated the highest expression levels in spleen, followed by liver and brain with particularly high levels in cortex and striatum [66]. Furthermore, P_2Y_{13} receptors were revealed in rat spinal cord, dorsal root ganglion [67], superior cervical ganglion [68] and mouse motor nerve terminals [11]. In latter case, Gi protein-coupled P_2Y_{13} receptors are considered as the best candidates for ATP/ADP-dependent negative feedback control of ACh release in the mammalian NMJs [11, 17].

ATP is one of the most common co-transmitters in both central and peripheral nervous system. In the synaptic cleft it is enzymatically hydrolyzed to ADP, AMP and finally adenosine [7, 8]. In addition, contracting muscle fibers [69, 70] and Schwann cells [71, 72] could be sources of extracellular purines. Both extracellular adenosine and ATP/ADP mainly reduce neurotransmitter release via binding to adenosine-and P_2Y-receptors in the amphibian and mammalian NMJs [11, 16, 40, 73–76].

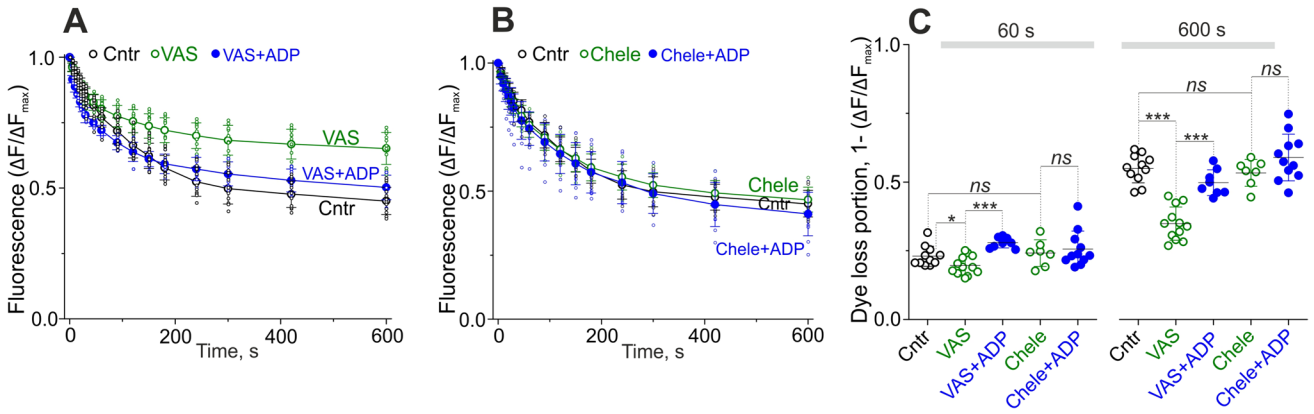

Fig. 5 Involvement of NADPH oxidase and protein kinase C in the effect of ADP on the rate of exocytotic FM-dye release during prolonged 20 Hz stimulation of phrenic nerve. **A**, **B** The kinetics of FM1-43 dye release from nerve terminals during stimulation after inhibition of NOX (A) or PKC (B) with VAS2870 (VAS) or chelerythrine (Chele), respectively. n = 12 (VAS), 8 (VAS + ADP), 8 (Chele) and 12 (Chele + ADP). Control curve is also shown on A and B (from Fig. 2A). **C** Quantification of FM1-43 dye loss for 60 and 600 s of the unloading stimulation under conditions of NOX or PKC blockage. n = 8–12 *per* group. *P < 0.05, ***P < 0.001—by a Mann–Whitney *U* test between groups; ns Non significant

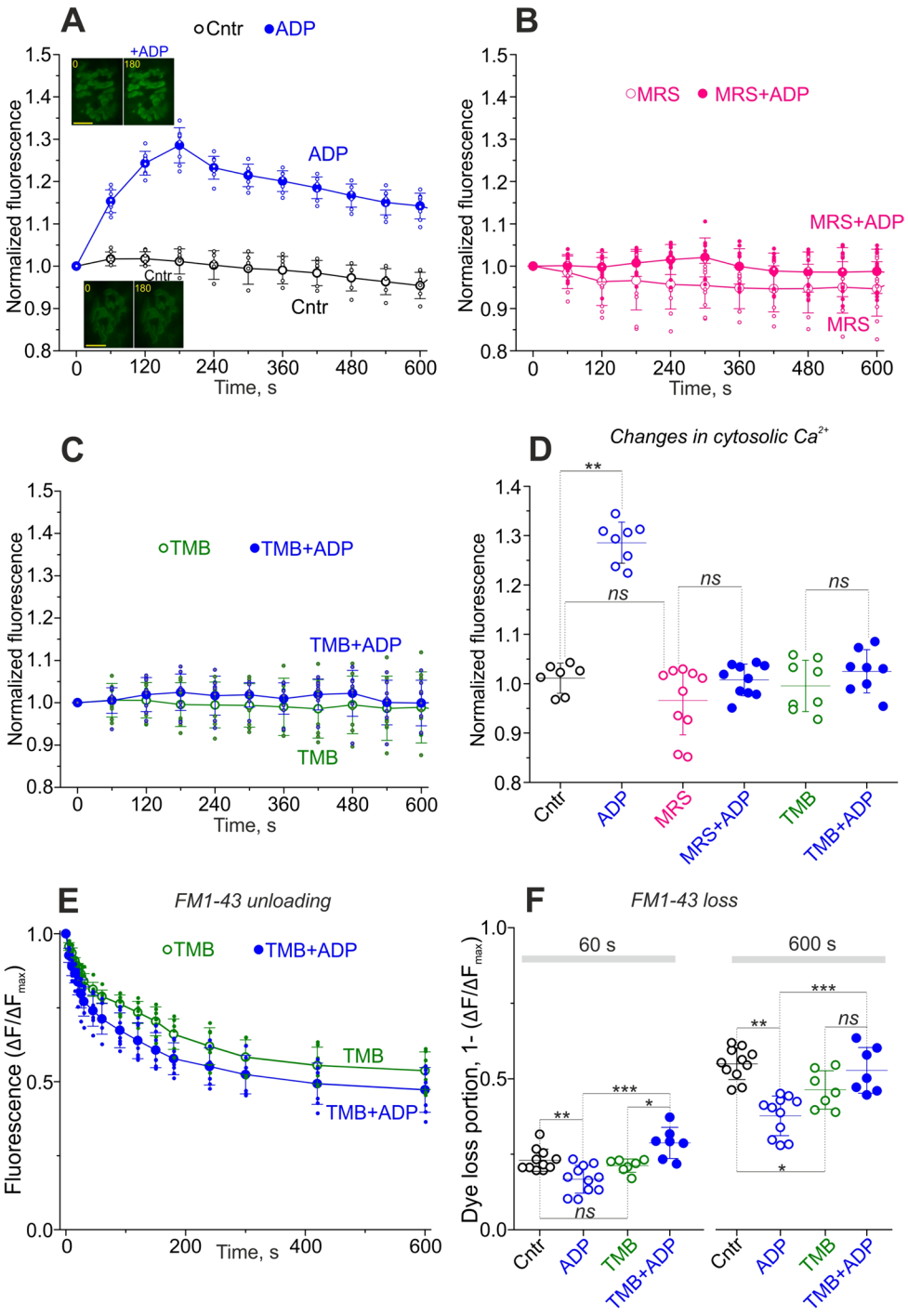

Fig. 6 P_2Y_{13} receptor-dependent changes in cytosolic calcium in synaptic regions. **A**–**C** Time course of Oregon Green 488 BAPTA-1 fluorescence (Ca^{2+} indicator) in synaptic regions in control (Cntr), after addition of ADP, MRS 2211 (MRS), TMB8 and ADP in combination with MRS 2211 or TMB8. **A**: insert, typical fluorescent images before (0) and 180 s after ADP/vehicle application; scale bars—15 µm. n = 7 (Cntr), 8 (ADP), 10 (MRS), 10 (MRS + ADP), 8 (TMB) and 8 (TMB + ADP). **D** Quantification of fluorescence changes by 180 s of the chemical application. **E** FM1-43 unloading curves in TMB and TMB + ADP-treated NMJs. n = 7 *per* group. **F** Quantification of FM1-43 portion loss after 60 and 600 s of stimulation at 20 Hz. D, F: *P < 0.05, **P < 0.01, ***P < 0.001—by a Mann–Whitney *U* test between groups; ns Non significant. **A**–**F**: data are represented as mean ± SD

Consistent with previous studies [11, 17], we showed that ADP and IDP reduce spontaneous exocytosis and evoked neurotransmitter release in response to low frequency stimulation in the mouse NMJs. In addition, experiments with tracking of exocytotic FM dye release demonstrated that ADP decreases the rate of exocytosis during intense activity. A selective antagonist of P_2Y_{13} receptors suppressed these effects of purinergic agonists, thereby pointing to P_2Y_{13} receptors as a main target for extracellular purines in the mouse NMJs. Importantly, the amplitude and kinetics of MEPCs were not affected, suggesting a pure presynaptic action of purinergic agonists.

The levels of endogenous purines at low frequency activity are not enough to regulate neurotransmitter release. Only induction of massive SV exocytosis seems to cause an elevation of endogenous purines concentration above purinergic receptor activation threshold [48]. Indeed, inhibitor of P_2Y_{13} receptors enhanced the rate of FM1-43 dye release during

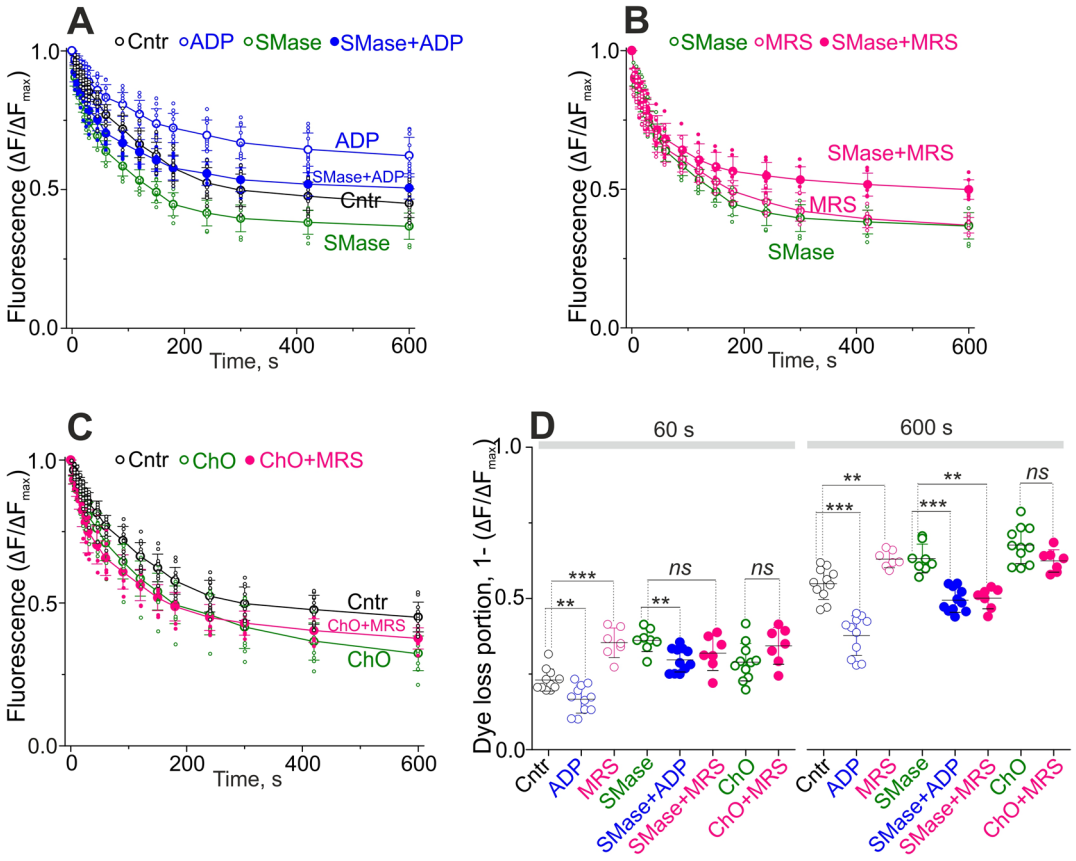

Fig. 7 The role of lipid microenvironment in purinergic regulation of exocytotic release at 20 Hz activity. **A**–**C** influence of ADP (**A**) and P_2Y_{13} antagonist MRS 2211 (**B**, **C**) on the kinetics of FM1-43 unloading after pretreatment with sphingomyelinase (**A**, **B**) or cholesterol oxidase (**C**). The unloading was induced by phrenic nerve stimulation. Control (Cntr), ADP and MRS curves from Fig. 2A, B are also shown. n = 9 (SMase), 12 (SMase + ADP), 8 (SMase + MRS), 12 (ChO) and 8 (ChO + MRS). **D** Quantification of FM1-43 dye portion released for 60 and 600 s of stimulation at 20 Hz. **P < 0.05, ***P < 0.001—by a Mann–Whitney *U* test between groups; ns non significant. **A**–**D**: data are represented as mean ± SD

nerve stimulation at 20 Hz, a more physiological mode of activity for phrenic motoneurons [43]. This points to suppression of SV involvement in exocytosis at intense activity due to activation of P_2Y_{13} receptors by endogenous purines.

ROS as Second Messengers in ADP Action in the NMJs

Activation of P_2Y receptors can lead to production of ROS as well as reactive nitrogen species, which affect multiple redox-dependent processes in cells [77, 78]. In the frog NMJs, ROS play a key role in P_2Y_{12} receptor-dependent action of ATP on neurotransmitter release [9, 13].

Previously, it was shown that phrenic nerve stimulation significantly increases extracellular concentrations of ATP [69, 79], which can activate P_2Y_{13} receptors at the mouse NMJs [48]. Here we demonstrated that both exogenous ADP and phrenic nerve activation increase intracellular ROS to comparable levels. In addition, estimation of extracellular levels of H_2O_2, the main signaling form of ROS [49–51], revealed an elevation of H_2O_2 generation upon both ADP application and phrenic nerve stimulation. This increase in H_2O_2 production was precluded by PTX, suggesting an involvement of Gi protein-coupled P_2Y_{13} receptors [11, 65].

High K^+ induces depolarization of the nerve terminals, causing quantal release of ACh and ATP [17, 80]. As a result, ATP/ADP and adenosine in the synaptic cleft can activate different purinergic receptors, particularly P_2Y_{13} and A_1, A_{2A} and A_3 subtypes [17]. We found that, similar to nerve stimulation, high K^+-induced membrane depolarization increases external H_2O_2 levels. This enhancement of H_2O_2 generation was markedly attenuated by P_2Y_{13} receptor antagonist. It is important to emphasize that the detected changes in H_2O_2 concentration correlate well with the physiological range of hydrogen peroxide amounts [81].

Main sources of O_2^- and H_2O_2 in cells are transmembrane NOXs and electron transport chain of mitochondria [82, 83]. NOXs also can be associated with specialized

endosomes (redoxosomes), this allows to compartmentalize H_2O_2-mediated signaling [84]. We found that ADP-induced H_2O_2 production in the neuromuscular preparations was completely blocked by VAS 2870, a specific NOX blocker [85]. In addition, VAS 2870 markedly attenuated ADP-mediated reduction of evoked ACh release in response to single stimuli and prevented ADP-induced suppression of exocytic FM1-43 dye loss during intense activity. These data suggest a key role of NOX-derived ROS in P_2Y_{13} receptor-dependent regulation of neuromuscular transmission. Indeed, antioxidants, NAC [86] and catalase [87], decreased the effect of ADP on neurotransmitter release. Note that catalase does not penetrate into cells, hence it should mainly neutralize extracellular H_2O_2, which is produced by plasma membrane bound NOXs [88].

In microglia and astrocytes, activation of P_2Y_{12} and P_2Y_{13} receptors caused Ca^{2+} mobilization [64, 89]. In mammalian NMJs, Gi protein-dependent Ca^{2+} release from intracellular store can increase H_2O_2 production [32]. We also found that ADP causes an increase in cytosolic Ca^{2+} (with the peak within 2–3 min) which is prevented by both P_2Y_{13} receptor antagonist (MRS 2211) and blocker of Ca^{2+} mobilization from endoplasmic reticulum (TMB8). Importantly, the elevation of $[Ca^{2+}]_{in}$ occurred before increase in intracellular ROS levels. Like NOX antagonist, inhibition of Ca^{2+} mobilization precluded suppressive action of ADP on the rate of exocytosis during intense activity. Accordingly, P_2Y_{13} receptor-dependent Ca^{2+}mobilization can contribute to NOX activation and suppression of exocytosis.

Increase in cytosolic Ca^{2+} can promote activation of NOX via Ca^{2+}-dependent signaling pathways engaging multiple players, e.g. PKC, MAP kinase or phospholipase A_2 [90]. P_2Y receptor-mediated Ca^{2+} mobilization is able to activate NOX2 through PKC in the immune cells [91]. We found that blocker of PKC, chelerythrine, acting in a similar manner as antioxidants and NOX inhibitor, suppresses ADP-induced decrease in evoked neurotransmitter release at low frequency stimulation. Furthermore, chelerythrine precluded ADP-induced changes in the rate of SV exocytosis at intense activity. Hence, P_2Y_{13} receptor-dependent attenuation of synaptic transmission can rely on Gi protein/Ca^{2+}/PKC/NOX/ROS signaling in the mouse NMJs.

G protein-coupled receptors as well as signaling molecules, including NOXs, can reside in the cholesterol and sphingomyelin-rich microdomains [9, 92, 93], which are likely to be abundant at the NMJs [22, 24, 94]. Previously, we found that exposure to SMase or ChO causes a partial lipid raft disruption and it increases the rate of SV exocytosis during intense activity at the diaphragm NMJs [30, 31]. Furthermore, the effect of SMase on neurotransmission was sensitive to Gi protein inhibition [30]. This suggests that lipid raft disruption might enhance neurotransmitter release by interfering with signaling via Gi protein-coupled receptors. Particularly, one of the reasons for the enhancement of neurotransmission can be attenuation of P_2Y_{13} receptor-dependent negative feedback regulation of exocytosis. Consistent with this hypothesis is that after ChO and SMase pretreatment blockage of P_2Y_{13} receptors lost its ability to enhance the rate of SV exocytosis at intense activity. In addition, SMase pretreatment inhibited the effects of exogenous ADP on evoked SV exocytosis and intracellular ROS levels. Hence, lipid-raft disrupting manipulations blunted ADP/P_2Y_{13} receptor-mediated suppression of neurotransmission in the mouse NMJs. Similarly, cholesterol depletion reduced and largely delayed the action of ATP via P_2Y_{12} receptors at the frog NMJs [9].

Interestingly, after exposure to SMase inhibition of P_2Y_{13} receptors caused the opposite effect, i.e. a decrease in the exocytotic rate at intense activity. Speculatively, changes in lipid microenvironment and (or) ceramide accumulation after sphingomyelin hydrolysis can lead to a switching of P_2Y_{13} receptor-dependent signaling to Gs protein. The latter can trigger cascades causing an increase in synaptic vesicle exocytosis [95, 96]. Although P_2Y_{13} receptors are mainly coupled to Gi protein, under some conditions, they can trigger signaling via Gs proteins [63, 97, 98]. Recently, we found that plasmalemmal sphingomyelin hydrolysis inverses the effects of β2-adrenergic agonist on neuromuscular transmission via switching to Gi protein-dependent signaling [99]. Thus, destabilization of lipid rafts and sphingomyelin hydrolysis can strongly interfere with both para-and endocrinal mechanisms of neurotransmission control, thereby contributing to the progression of neuromuscular disorders.

Lipid raft disruption in the NMJs can occur at the early stages in amyotrophic lateral sclerosis [27, 28] and during short-term muscle disuse [25], whereas overexpression of a lipid raft organizer protein caveolin had beneficial actions in models of amyotrophic lateral sclerosis [100, 101]. Furthermore, upregulation of SMase was demonstrated in conditions associated with skeletal muscle atrophy and damage [102–106]. According to this scenario, loss of the negative feedback control mechanism can lead to excessive neurotransmission and ACh release. Higher levels of ACh at the synaptic cleft may promote the degeneration of adult NMJs, contributing to disease-related deteriorations of motor function [6]. By contrast, increased neurotransmitter release can also be a compensatory response to keep the safety factor of neuromuscular transmission at the required level under pathological conditions or during aging [107]. In addition, activity of nicotinic ACh receptors can counteract muscle fiber atrophy and favor reinnervation [108].

Conclusions

Co-transmitter ATP and its derivatives mediate a negative feedback loop that limits excessive ACh release in the mammalian NMJs. Our data indicates that ATP/ADP, via activation of the P_2Y_{13} receptor, triggers sequential Ca^{2+} mobilization and NOX-dependent ROS production. Generated ROS (particularly H_2O_2) attenuate SV exocytosis induced by both low and higher frequency stimulation of the phrenic nerve. Targeting key components of lipid rafts suppresses P_2Y_{13} receptor-mediated effects on both exocytosis and ROS levels, pointing to the key meaning of lipid microenvironment for purinergic modulation of neuromuscular transmission.

Acknowledgements We thank Dr. Zakharov A.V. for technical assistance; AMP was supported by assignment for Kazan Institute of Biochemistry and Biophysics, FRC Kazan Scientific Center of Russian Academy of Sciences.

Author Contributions ARG: electrophysiological and ROS detection experiments, visualization, and data analysis, writing, review & editing; KAM: fluorescent experiments (FM-dye and calcium imaging), visualization, and data analysis; AMP: funding acquisition, conceptualization; writing, review & editing. All authors have read and agreed to the published version of the manuscript.

Funding This work was supported by the by Russian Science Foundation, grant number [21-14-00044], https://rscf.ru/project/21-14-00044/, (#3.1, 3.2, 3.4, 3.7 result's sections), and [23-75-10022] https://www.rscf.ru/project/23-75-10022/ (#3.3, 3.5, 3.6 result's section).

Data Availability All mentioned data are represented in the main manuscript figures. Other additional data will be made available on reasonable request.

Declarations

Competing Interests The authors declare that they have no competing interests.

Ethical Approval The experimental protocol met the requirements of the EU Directive 2010/63/EU and was approved by the Local Ethical Committee of Kazan Federal Scientific Centre (#23/7; May 12, 2023) and Kazan Medical University (Protocol #1/January 25, 2022). The current study was conducted in compliance with the NIH Guide for the Care and Use of Laboratory Animals.

Consent for Publication Not applicable.

References

1. Wood SJ, Slater CR (2001) Safety factor at the neuromuscular junction. Prog Neurobiol 64:393–429
2. Slater CR (2015) The functional organization of motor nerve terminals. Prog Neurobiol 134:55–103
3. Petrov AM, Giniatullin AR, Sitdikova GF, Zefirov AL (2008) The role of cGMP-dependent signaling pathway in synaptic vesicle cycle at the frog motor nerve terminals. J Neurosci 28:13216–13222
4. Wu LG, Betz WJ (1998) Kinetics of synaptic depression and vesicle recycling after tetanic stimulation of frog motor nerve terminals. Biophys J 74:3003–3009
5. Harris JJ, Jolivet R, Attwell D (2012) Synaptic energy use and supply. Neuron 75:762–777
6. Sugita S, Fleming LL, Wood C, Vaughan SK, Gomes MP, Camargo W, Naves LA, Prado VF, Prado MA, Guatimosim C, Valdez G (2016) VAChT overexpression increases acetylcholine at the synaptic cleft and accelerates aging of neuromuscular junctions. Skelet Muscle 6:31
7. Burnstock G (2009) Purinergic cotransmission. Exp Physiol 94:20–24
8. Sousa-Soares C, Noronha-Matos JB, Correia-de-Sa P (2023) Purinergic tuning of the tripartite neuromuscular synapse. Mol Neurobiol 60:4084–4104
9. Giniatullin A, Petrov A, Giniatullin R (2015) The involvement of P2Y12 receptors, NADPH oxidase, and lipid rafts in the action of extracellular ATP on synaptic transmission at the frog neuromuscular junction. Neuroscience 285:324–332
10. Sokolova E, Grishin S, Shakirzyanova A, Talantova M, Giniatullin R (2003) Distinct receptors and different transduction mechanisms for ATP and adenosine at the frog motor nerve endings. Eur J Neurosci 18:1254–1264
11. Guarracino JF, Cinalli AR, Fernandez V, Roquel LI, Losavio AS (2016) P2Y13 receptors mediate presynaptic inhibition of acetylcholine release induced by adenine nucleotides at the mouse neuromuscular junction. Neuroscience 326:31–44
12. Tsentsevitsky AN, Petrov AM (2022) L-type Ca(2+) channels at low external calcium differentially regulate neurotransmitter release in proximal-distal compartments of the frog neuromuscular junction. Cell Mol Neurobiol 42:2833–2847
13. Giniatullin AR, Grishin SN, Sharifullina ER, Petrov AM, Zefirov AL, Giniatullin RA (2005) Reactive oxygen species contribute to the presynaptic action of extracellular ATP at the frog neuromuscular junction. J Physiol 565:229–242
14. Giniatullin AR, Darios F, Shakirzyanova A, Davletov B, Giniatullin R (2006) SNAP25 is a pre-synaptic target for the depressant action of reactive oxygen species on transmitter release. J Neurochem 98:1789–1797
15. Tsentsevitsky AN, Zakyrjanova GF, Petrov AM (2020) Cadmium desynchronizes neurotransmitter release in the neuromuscular junction: key role of ROS. Free Radic Biol Med 155:19–28
16. Tsentsevitsky AN, Gafurova CR, Petrov AM (2022) K(ATP) channels as ROS-dependent modulator of neurotransmitter release at the neuromuscular junctions. Life Sci 310:121120
17. Guarracino JF, Cinalli AR, Veggetti MI, Losavio AS (2018) Endogenous purines modulate K(+)-evoked ACh secretion at the mouse neuromuscular junction. J Neurosci Res 96:1066–1079
18. Lichtenstein L, Serhan N, Espinosa-Delgado S, Fabre A, Annema W, Tietge UJ, Robaye B, Boeynaems JM, Laffargue M, Perret B, Martinez LO (2015) Increased atherosclerosis in P2Y13/apolipoprotein E double-knockout mice: contribution of P2Y13 to reverse cholesterol transport. Cardiovasc Res 106:314–323
19. Goffinet M, Tardy C, Boubekeur N, Cholez G, Bluteau A, Oniciu DC, Lalwani ND, Dasseux JL, Barbaras R, Baron R (2014) P2Y13 receptor regulates HDL metabolism and atherosclerosis in vivo. PLoS ONE 9:e95807
20. Voss U, Turesson MF, Robaye B, Boeynaems JM, Olde B, Erlinge D, Ekblad E (2014) The enteric nervous system of P2Y13 receptor null mice is resistant against high-fat-diet- and palmitic-acid-induced neuronal loss. Purinergic Signal 10:455–464
21. Marchand S, Devillers-Thiery A, Pons S, Changeux JP, Cartaud J (2002) Rapsyn escorts the nicotinic acetylcholine receptor along the exocytic pathway via association with lipid rafts. J Neurosci 22:8891–8901

22. Petrov AM, Kudryashova KE, Odnoshivkina YG, Zefirov AL (2011) Cholesterol and lipid rafts in the plasma membrane of nerve terminal and membrane of synaptic vesicles. Neurochem J 5:13–19
23. Gonzalez Porras MA, Fogarty MJ, Gransee HM, Sieck GC, Mantilla CB (2019) Frequency-dependent lipid raft uptake at rat diaphragm muscle axon terminals. Muscle Nerve 59:611–618
24. Kwan HR, Chan ZC, Bi X, Kutkowska J, Proszynski TJ, Chan CB, Lee CW (2023) Nerve-independent formation of membrane infoldings at topologically complex postsynaptic apparatus by caveolin-3. Sci Adv. https://doi.org/10.1126/sciadv.adg0183
25. Petrov AM, Kravtsova VV, Matchkov VV, Vasiliev AN, Zefirov AL, Chibalin AV, Heiny JA, Krivoi II (2017) Membrane lipid rafts are disturbed in the response of rat skeletal muscle to short-term disuse. Am J Physiol Cell Physiol 312:C627–C637
26. Bryndina IG, Shalagina MN, Sekunov AV, Zefirov AL, Petrov AM (2018) Clomipramine counteracts lipid raft disturbance due to short-term muscle disuse. Neurosci Lett 664:1–6
27. Zakyrjanova GF, Giniatullin AR, Mukhutdinova KA, Kuznetsova EA, Petrov AM (2021) Early differences in membrane properties at the neuromuscular junctions of ALS model mice: effects of 25-hydroxycholesterol. Life Sci 273:119300
28. Mukhamedyarov MA, Khabibrakhmanov AN, Khuzakhmetova VF, Giniatullin AR, Zakirjanova GF, Zhilyakov NV, Mukhutdinova KA, Samigullin DV, Grigoryev PN, Zakharov AV, Zefirov AL, Petrov AM (2023) Early alterations in structural and functional properties in the neuromuscular junctions of mutant FUS mice. Int J Mol Sci. https://doi.org/10.3390/ijms24109022
29. Glavinovic MI (1979) Voltage clamping of unparalysed cut rat diaphragm for study of transmitter release. J Physiol 290:467–480
30. Tsentsevitsky AN, Gafurova CR, Mukhutdinova KA, Giniatullin AR, Fedorov NS, Malomouzh AI, Petrov AM (2023) Sphingomyelinase modulates synaptic vesicle mobilization at the mice neuromuscular junctions. Life Sci 318:121507
31. Zakirjanova GF, Giniatullin AR, Gafurova CR, Malomouzh AI, Fedorov NS, Khaziev AN, Tsentsevitsky AN, Petrov AM (2023) Effects of cholesterol oxidase on neurotransmission and acetylcholine levels at the mice neuromuscular junctions. Arch Biochem Biophys 749:109803
32. Zakyrjanova GF, Tsentsevitsky AN, Kuznetsova EA, Petrov AM (2021) Immune-related oxysterol modulates neuromuscular transmission via non-genomic liver X receptor-dependent mechanism. Free Radic Biol Med 174:121–134
33. Mukhutdinova KA, Kasimov MR, Giniatullin AR, Zakyrjanova GF, Petrov AM (2018) 24S-hydroxycholesterol suppresses neuromuscular transmission in SOD1(G93A) mice: a possible role of NO and lipid rafts. Mol Cell Neurosci 88:308–318
34. Giniatullin A, Petrov A, Giniatullin R (2019) Action of hydrogen peroxide on synaptic transmission at the mouse neuromuscular junction. Neuroscience 399:135–145
35. Zakharov AV (2019) Elph: an open-source program for acquisition control and analysis of electrophysiological signals. Uchenye Zapiski Kazanskogo Universiteta Seriya Estestvennye Nauki 161:245–254
36. Kasimov MR, Fatkhrakhmanova MR, Mukhutdinova KA, Petrov AM (2017) 24S-Hydroxycholesterol enhances synaptic vesicle cycling in the mouse neuromuscular junction: Implication of glutamate NMDA receptors and nitric oxide. Neuropharmacology 117:61–73
37. Betz WJ, Bewick GS (1992) Optical analysis of synaptic vesicle recycling at the frog neuromuscular junction. Science 255:200–203
38. Oparka M, Walczak J, Malinska D, van Oppen L, Szczepanowska J, Koopman WJH, Wieckowski MR (2016) Quantifying ROS levels using CM-H(2)DCFDA and HyPer. Methods 109:3–11
39. Kalyanaraman B, Darley-Usmar V, Davies KJ, Dennery PA, Forman HJ, Grisham MB, Mann GE, Moore K, Roberts LJ, Ischiropoulos H (2012) Measuring reactive oxygen and nitrogen species with fluorescent probes: challenges and limitations. Free Radic Biol Med 52:1–6
40. De Lorenzo S, Veggetti M, Muchnik S, Losavio A (2006) Presynaptic inhibition of spontaneous acetylcholine release mediated by P2Y receptors at the mouse neuromuscular junction. Neuroscience 142:71–85
41. Zhang FL, Luo L, Gustafson E, Palmer K, Qiao X, Fan X, Yang S, Laz TM, Bayne M, Monsma F Jr (2002) P2Y(13): identification and characterization of a novel Galphai-coupled ADP receptor from human and mouse. J Pharmacol Exp Ther 301:705–713
42. Malin SA, Molliver DC (2010) Gi-and Gq-coupled ADP (P2Y) receptors act in opposition to modulate nociceptive signaling and inflammatory pain behavior. Mol Pain 6:21
43. Lee KZ, Fuller DD (2011) Neural control of phrenic motoneuron discharge. Respir Physiol Neurobiol 179:71–79
44. Gafurova CR, Tsentsevitsky AN, Petrov AM (2022) Frequency-dependent engagement of synaptic vesicle pools in the mice motor nerve terminals. Cell Mol Neurobiol. https://doi.org/10.1007/s10571-022-01202-x
45. Richards DA, Guatimosim C, Rizzoli SO, Betz WJ (2003) Synaptic vesicle pools at the frog neuromuscular junction. Neuron 39:529–541
46. Rizzoli SO, Betz WJ (2005) Synaptic vesicle pools. Nat Rev Neurosci 6:57–69
47. Delgado R, Maureira C, Oliva C, Kidokoro Y, Labarca P (2000) Size of vesicle pools, rates of mobilization, and recycling at neuromuscular synapses of a *Drosophila* mutant, shibire. Neuron 28:941–953
48. Gonzalez Sanabria J, Hurtado Paso M, Frontera T, Losavio A (2022) Effect of endogenous purines on electrically evoked ACh release at the mouse neuromuscular junction. J Neurosci Res 100:1933–1950
49. Sies H (2014) Role of metabolic H2O2 generation: redox signaling and oxidative stress. J Biol Chem 289:8735–8741
50. Holmstrom KM, Finkel T (2014) Cellular mechanisms and physiological consequences of redox-dependent signalling. Nat Rev Mol Cell Biol 15:411–421
51. Winterbourn CC (2018) Biological production, detection, and fate of hydrogen peroxide. Antioxid Redox Signal 29:541–551
52. Augsburger F, Filippova A, Jaquet V (2019) Methods for detection of NOX-derived superoxide radical anion and hydrogen peroxide in cells. Methods Mol Biol 1982:233–241
53. Rastogi R, Geng X, Li F, Ding Y (2016) NOX activation by subunit interaction and underlying mechanisms in disease. Front Cell Neurosci 10:301
54. Cooke M, Zhang S, Cornejo Maciel F, Kazanietz MG (2023) Gi/o GPCRs drive the formation of actin-rich tunneling nanotubes in cancer cells via a Gbetagamma/PKCalpha/FARP1/Cdc42 axis. J Biol Chem 299:104983
55. Prakasam HS, Gallo LI, Li H, Ruiz WG, Hallows KR, Apodaca G (2014) A1 adenosine receptor-stimulated exocytosis in bladder umbrella cells requires phosphorylation of ADAM17 Ser-811 and EGF receptor transactivation. Mol Biol Cell 25:3798–3812
56. Jiang F, Zhang Y, Dusting GJ (2011) NADPH oxidase-mediated redox signaling: roles in cellular stress response, stress tolerance, and tissue repair. Pharmacol Rev 63:218–242
57. Jiang XC, Li Z (2022) Sphingolipids and Cholesterol. Adv Exp Med Biol 1372:1–14
58. Nguyen DH, Taub DD (2003) Inhibition of chemokine receptor function by membrane cholesterol oxidation. Exp Cell Res 291:36–45

59. Gniadecki R (2004) Depletion of membrane cholesterol causes ligand-independent activation of Fas and apoptosis. Biochem Biophys Res Commun 320:165–169
60. Yu C, Alterman M, Dobrowsky RT (2005) Ceramide displaces cholesterol from lipid rafts and decreases the association of the cholesterol binding protein caveolin-1. J Lipid Res 46:1678–1691
61. Horres CR, Hannun YA (2012) The roles of neutral sphingomyelinases in neurological pathologies. Neurochem Res 37:1137–1149
62. Burnstock G, Krugel U, Abbracchio MP, Illes P (2011) Purinergic signalling: from normal behaviour to pathological brain function. Prog Neurobiol 95:229–274
63. Communi D, Gonzalez NS, Detheux M, Brezillon S, Lannoy V, Parmentier M, Boeynaems JM (2001) Identification of a novel human ADP receptor coupled to G(i). J Biol Chem 276:41479–41485
64. Perez-Sen R, Queipo MJ, Morente V, Ortega F, Delicado EG, Miras-Portugal MT (2015) Neuroprotection Mediated by P2Y13 nucleotide receptors in neurons. Comput Struct Biotechnol J 13:160–168
65. Jacobson KA, Delicado EG, Gachet C, Kennedy C, von Kugelgen I, Li B, Miras-Portugal MT, Novak I, Schoneberg T, Perez-Sen R, Thor D, Wu B, Yang Z, Muller CE (2020) Update of P2Y receptor pharmacology: IUPHAR Review 27. Br J Pharmacol 177:2413–2433
66. Fumagalli M, Trincavelli L, Lecca D, Martini C, Ciana P, Abbracchio MP (2004) Cloning, pharmacological characterisation and distribution of the rat G-protein-coupled P2Y(13) receptor. Biochem Pharmacol 68:113–124
67. Heinrich A, Kittel A, Csolle C, Sylvester Vizi E, Sperlagh B (2008) Modulation of neurotransmitter release by P2X and P2Y receptors in the rat spinal cord. Neuropharmacology 54:375–386
68. Yin S, Yang X, Li H, Li C, Li C, Chen C, Ye S, Zou L, Liang S, Liu S (2024) P2Y(13) receptor involved in HIV-1 gp120 induced neuropathy in superior cervical ganglia through NLRP3 inflammasome activation. Neuropharmacology 245:109818
69. Santos DA, Salgado AI, Cunha RA (2003) ATP is released from nerve terminals and from activated muscle fibres on stimulation of the rat phrenic nerve. Neurosci Lett 338:225–228
70. Smith DO (1991) Sources of adenosine released during neuromuscular transmission in the rat. J Physiol 432:343–354
71. Liu GJ, Werry EL, Bennett MR (2005) Secretion of ATP from Schwann cells in response to uridine triphosphate. Eur J Neurosci 21:151–160
72. Todd KJ, Robitaille R (2006) Purinergic modulation of synaptic signalling at the neuromuscular junction. Pflugers Arch 452:608–614
73. Schwartz AD, Whitacre CL, Lin Y, Wilson DF (2003) Adenosine inhibits N-type calcium channels at the rat neuromuscular junction. Clin Exp Pharmacol Physiol 30:174–177
74. Ginsborg BL, Hirst GD (1972) The effect of adenosine on the release of the transmitter from the phrenic nerve of the rat. J Physiol 224:629–645
75. Bennett MR, Karunanithi S, Lavidis NA (1991) Probabilistic secretion of quanta from nerve terminals in toad (Bufo marinus) muscle modulated by adenosine. J Physiol 433:421–434
76. Ribeiro JA, Walker J (1975) The effects of adenosine triphosphate and adenosine diphosphate on transmission at the rat and frog neuromuscular junctions. Br J Pharmacol 54:213–218
77. Savio LEB, Leite-Aguiar R, Alves VS, Coutinho-Silva R, Wyse ATS (2021) Purinergic signaling in the modulation of redox biology. Redox Biol 47:102137
78. Shen JZ, Zheng XF, Kwan CY (2000) Evidence for P(2)-purinoceptors contribution in H(2)O(2)-induced contraction of rat aorta in the absence of endothelium. Cardiovasc Res 47:574–585
79. Vizi ES, Nitahara K, Sato K, Sperlagh B (2000) Stimulation-dependent release, breakdown, and action of endogenous ATP in mouse hemidiaphragm preparation: the possible role of ATP in neuromuscular transmission. J Auton Nerv Syst 81:278–284
80. Liley AW (1956) The effects of presynaptic polarization on the spontaneous activity at the mammalian neuromuscular junction. J Physiol 134:427–443
81. Huang BK, Sikes HD (2014) Quantifying intracellular hydrogen peroxide perturbations in terms of concentration. Redox Biol 2:955–962
82. Bedard K, Krause KH (2007) The NOX family of ROS-generating NADPH oxidases: physiology and pathophysiology. Physiol Rev 87:245–313
83. Murphy MP (2009) How mitochondria produce reactive oxygen species. Biochem J 417:1–13
84. Spencer NY, Engelhardt JF (2014) The basic biology of redoxosomes in cytokine-mediated signal transduction and implications for disease-specific therapies. Biochemistry 53:1551–1564
85. Altenhofer S, Radermacher KA, Kleikers PW, Wingler K, Schmidt HH (2015) Evolution of NADPH oxidase inhibitors: selectivity and mechanisms for target engagement. Antioxid Redox Signal 23:406–427
86. Sahasrabudhe SA, Terluk MR, Kartha RV (2023) N-acetylcysteine pharmacology and applications in rare diseases-repurposing an old antioxidant. Antioxidants (Basel). https://doi.org/10.3390/antiox12071316
87. Galasso M, Gambino S, Romanelli MG, Donadelli M, Scupoli MT (2021) Browsing the oldest antioxidant enzyme: catalase and its multiple regulation in cancer. Free Radic Biol Med 172:264–272
88. Wang Y, Branicky R, Noe A, Hekimi S (2018) Superoxide dismutases: dual roles in controlling ROS damage and regulating ROS signaling. J Cell Biol 217:1915–1928
89. Ming LG, Hu DX, Zuo C, Zhang WJ (2023) G protein-coupled P2Y12 receptor is involved in the progression of neuropathic pain. Biomed Pharmacother 162:114713
90. Gordeeva AV, Zvyagilskaya RA, Labas YA (2003) Cross-talk between reactive oxygen species and calcium in living cells. Biochemistry (Mosc) 68:1077–1080
91. Guerra AN, Gavala ML, Chung HS, Bertics PJ (2007) Nucleotide receptor signalling and the generation of reactive oxygen species. Purinergic Signal 3:39–51
92. Vilhardt F, van Deurs B (2004) The phagocyte NADPH oxidase depends on cholesterol-enriched membrane microdomains for assembly. EMBO J 23:739–748
93. Da N, Volonte C (2013) Metabotropic purinergic receptors in lipid membrane microdomains. Curr Med Chem 20:56–63
94. Stetzkowski-Marden F, Recouvreur M, Camus G, Cartaud A, Marchand S, Cartaud J (2006) Rafts are required for acetylcholine receptor clustering. J Mol Neurosci 30:37–38
95. Polishchuk A, Cilleros-Mane V, Just-Borras L, Balanya-Segura M, Vandellos Pont G, Silvera Simon C, Tomas M, Garcia N, Tomas J, Lanuza MA (2023) Synaptic retrograde regulation of the PKA-induced SNAP-25 and Synapsin-1 phosphorylation. Cell Mol Biol Lett 28:17
96. Losavio A, Muchnik S (2000) Facilitation of spontaneous acetylcholine release induced by activation of cAMP in rat neuromuscular junctions. Life Sci 66:2543–2556
97. Perez-Sen R, Gomez-Villafuertes R, Ortega F, Gualix J, Delicado EG, Miras-Portugal MT (2017) An update on P2Y13 receptor signalling and function. Adv Exp Med Biol 1051:139–168
98. Marteau F, Le Poul E, Communi D, Communi D, Labouret C, Savi P, Boeynaems JM, Gonzalez NS (2003) Pharmacological characterization of the human P2Y13 receptor. Mol Pharmacol 64:104–112

99. Gafurova CR, Tsentsevitsky AN, Fedorov NS, Khaziev AN, Malomouzh AI, Petrov AM (2024) beta2-adrenergic regulation of the neuromuscular transmission and its lipid-dependent switch. Mol Neurobiol. https://doi.org/10.1007/s12035-024-03991-2
100. Wang S, Ichinomiya T, Savchenko P, Wang D, Sawada A, Li X, Duong T, Li W, Bonds JA, Kim EJ, Miyanohara A, Roth DM, Patel HH, Patel PM, Tadokoro T, Marsala M, Head BP (2022) Subpial delivery of adeno-associated virus 9-synapsin-caveolin-1 (AAV9-SynCav1) preserves motor neuron and neuromuscular junction morphology, motor function, delays disease onset, and extends survival in hSOD1(G93A) mice. Theranostics 12:5389–5403
101. Sawada A, Wang S, Jian M, Leem J, Wackerbarth J, Egawa J, Schilling JM, Platoshyn O, Zemljic-Harpf A, Roth DM, Patel HH, Patel PM, Marsala M, Head BP (2019) Neuron-targeted caveolin-1 improves neuromuscular function and extends survival in SOD1(G93A) mice. FASEB J 33:7545–7554
102. Empinado HM, Deevska GM, Nikolova-Karakashian M, Yoo JK, Christou DD, Ferreira LF (2014) Diaphragm dysfunction in heart failure is accompanied by increases in neutral sphingomyelinase activity and ceramide content. Eur J Heart Fail 16:519–525
103. Olsson K, Cheng AJ, Al-Ameri M, Tardif N, Melin M, Rooyackers O, Lanner JT, Westerblad H, Gustafsson T, Bruton JD, Rullman E (2022) Sphingomyelinase activity promotes atrophy and attenuates force in human muscle fibres and is elevated in heart failure patients. J Cachexia Sarcopenia Muscle 13:2551–2561
104. Petrov AM, Shalagina MN, Protopopov VA, Sergeev VG, Ovechkin SV, Ovchinina NG, Sekunov AV, Zefirov AL, Zakirjanova GF, Bryndina IG (2019) Changes in membrane ceramide pools in rat soleus muscle in response to short-term disuse. Int J Mol Sci. https://doi.org/10.3390/ijms20194860
105. Choi BJ, Park KH, Park MH, Huang EJ, Kim SH, Bae JS, Jin HK (2022) Acid sphingomyelinase inhibition improves motor behavioral deficits and neuronal loss in an amyotrophic lateral sclerosis mouse model. BMB Rep 55:621–626
106. Lee YI, Leem YH (2019) Acid sphingomyelinase inhibition alleviates muscle damage in gastrocnemius after acute strenuous exercise. J Exerc Nutrition Biochem 23:1–6
107. Camargo WL, Kushmerick C, Pinto E, Souza N, Cavalcante W, Souza-Neto FP, Guatimosim S, Prado M, Guatimosim C, Naves LA (2022) Homeostatic plasticity induced by increased acetylcholine release at the mouse neuromuscular junction. Neurobiol Aging 110:13–26
108. Cisterna BA, Vargas AA, Puebla C, Fernandez P, Escamilla R, Lagos CF, Matus MF, Vilos C, Cea LA, Barnafi E, Gaete H, Escobar DF, Cardozo CP, Saez JC (2020) Active acetylcholine receptors prevent the atrophy of skeletal muscles and favor reinnervation. Nat Commun 11:1073

Authors and Affiliations

Arthur R. Giniatullin[1] · Kamilla A. Mukhutdinova[1,2] · Alexey M. Petrov[1,2,3]

✉ Arthur R. Giniatullin
arthur.giniyatullin@kazangmu.ru

✉ Alexey M. Petrov
alexey.petrov@kazangmu.ru

[1] Kazan State Medical University, 49 Butlerova St., Kazan, RT, Russia 420012

[2] Laboratory of Biophysics of Synaptic Processes, Kazan Institute of Biochemistry and Biophysics, FRC Kazan Scientific Center of RAS, 2/31 Lobachevsky St, Kazan, RT, Russia 420111

[3] Kazan Federal University, 18 Kremlyovskaya Street, Kazan, Russia 420008